

SPITZER AND MAGELLAN OBSERVATIONS OF NGC 2264: A REMARKABLE STAR-FORMING CORE NEAR IRS 2

E. T. YOUNG,¹ P. S. TEIXEIRA,^{2,3} C. J. LADA,² J. MUZEROLLE,¹ S. E. PERSSON,⁴ D. C. MURPHY,⁴ N. SIEGLER,¹
M. MARENGO,² O. KRAUSE,¹ AND A. K. MAINZER⁵

Received 2005 November 4; accepted 2006 January 4

ABSTRACT

We analyze *Spitzer* and Magellan observations of a star-forming core near IRS 2 in the young cluster NGC 2264. The submillimeter source IRAS 12 S1, previously believed to be an intermediate-mass Class 0 object is shown to be a dense collection of embedded, low-mass stars. We argue that this group of stars represents the fragmenting collapse of a dense, turbulent core, using a number of indicators of extreme youth. With reasonable estimates for the velocity dispersion in the group, we estimate a dynamical lifetime of only a few times 10^4 yr. Spectral energy distributions of stars in the core are consistent with Class I or Class 0 assignments. We present observations of an extensive system of molecular hydrogen emission knots. The luminosity of the objects in the core region are consistent with roughly solar mass protostars.

Subject headings: open clusters and associations: individual (NGC 2264) — stars: formation — stars: pre-main-sequence

Online material: color figures

1. INTRODUCTION

Over the past 20 years, a relatively consistent picture of low-mass star formation has emerged. In this scenario, a dense molecular core becomes gravitationally unstable, collapses, and begins the process of star formation. We know, however, that real star formation is significantly more complex. In particular, stars do not form in isolation, and interactions between different protostars may be quite important in their development. Recent numerical simulations by Bate et al. (2003), for example, show that star formation in a turbulent core is a highly dynamic, interactive process. Because this early formation activity occurs in regions of very high obscuration, detailed investigations have been difficult given the limited sensitivity and angular resolution of available far infrared capabilities. The observational situation has dramatically improved with the launch of *Spitzer*.

NGC 2264 has long been one of the touchstones in star formation studies. Beginning with the work of Herbig (1954) and Walker (1956), studies at all available wavelengths have been conducted in this extremely young cluster. At a distance of 800 pc, NGC 2264 is close enough for detailed investigations of the stellar population down to very low masses. While more distant than some of the other well-studied star formation regions like ρ Ophiuchi or the Orion molecular cloud, NGC 2264 displays some of the best examples of the interaction of the interstellar medium with the young stars.

Investigators at optical wavelengths (Sung et al. 1997; Flaccomio et al. 1999; Park et al. 2000; Rebull et al. 2002; Dahm & Simon

2005) have fit their data to theoretical isochrones and find typical ages in the 1–3 Myr range for the young stellar population. They also find, however, that there is a wide range in derived ages for the individual stars, going from 10^5 to nearly 10^7 yr. The region contains numerous *Infrared Astronomical Satellite* (*IRAS*) sources, many of which have been classified as Class I protostars (Margulis et al. 1989). Moreover, the presence of Herbig-Haro objects, molecular outflows (Margulis et al. 1988; Wolf-Chase & Walker 1995), and Class I objects (Wolf-Chase et al. 2003) attest to continuing, active star formation.

One of these Class I sources, IRS 2 (listed as IRAS 06382+0939 in the *IRAS* Point Source Catalog) is located 17' south of the O7 star S Mon and 7' north of the Cone Nebula in a dense clump of molecular gas. It was identified as a source of far-infrared radiation by Sargent et al. (1984) and by Schwartz et al. (1985). Using the Kuiper Airborne Observatory, Cohen et al. (1985) found a second peak of far-infrared radiation 2' to the southwest. Castelaz & Grasdalen (1988) mapped the region at near-infrared wavelengths and associated IRS 2 with a pair of red nebulous objects (RNO-E and RNO-W). IRS 2 was designated as IRAS 12 by Margulis et al. (1989) in their *IRAS* survey of the NGC 2264 region, and they classified it as a likely Class I protostar. This classification was supported by the association of IRAS 12 with a high-velocity molecular outflow (NGC 2264 Flow D). More recently, this region has been mapped at higher angular resolution at submillimeter wavelengths by Williams & Garland (2002) and Wolf-Chase et al. (2003). Those maps show that the *IRAS* source itself is weak at 450 and 850 μm , but that it is part of a complex collection of submillimeter cores. The latter authors argue that these cores have a range of evolutionary stages.

Teixeira et al. (2006) presented *Spitzer* observations of NGC 2264 IRS 2 region. They found that bright 24 μm sources were aligned in a spokelike pattern appearing to emanate from IRAS 06382+0939 and coinciding with submillimeter dust filaments. In addition they found that the nearest neighbor spacing between these sources had a peak in the distribution of approximately 20'', very close to the Jeans length of the cloud. They argued

¹ Steward Observatory, University of Arizona, 933 North Cherry Avenue, Tucson, AZ 85721.

² Harvard-Smithsonian Center for Astrophysics, Mail Stop 42, 60 Garden Street, Cambridge, MA 02138.

³ Departamento de Física, Faculdade de Ciências de Universidade de Lisboa, Lisbon, Portugal.

⁴ Observatories of the Carnegie Institution of Washington, 813 Santa Barbara Street, Pasadena, CA 91101.

⁵ Jet Propulsion Laboratory, California Institute of Technology, 4800 Oak Grove Drive, Pasadena, CA 91109.

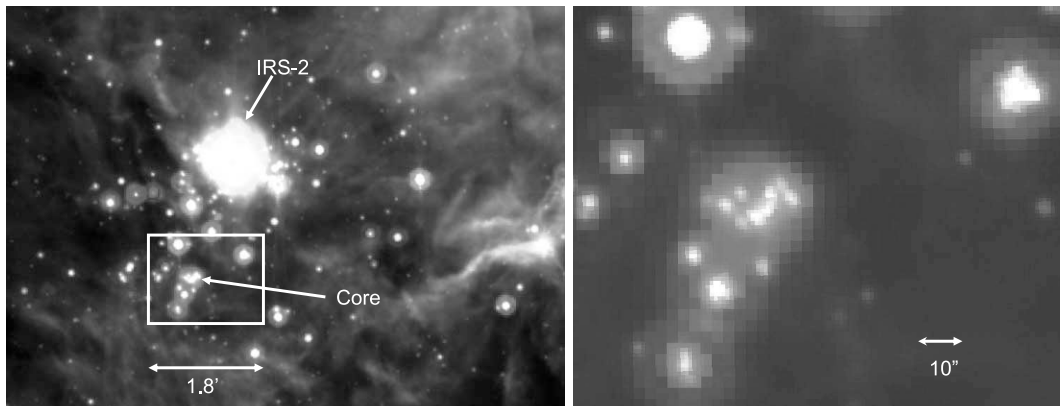


FIG. 1.—*Left*: Composite image of *Spitzer* observations of the NGC 2264 IRS 2 region using data from the 3.6, 8.0, and 24 μm bands. The image covers approximately $8'.1 \times 5'.8$. The coverage of the PANIC image is indicated by the box. The field center is (J2000.0) $6^{\text{h}}40^{\text{m}}56^{\text{s}}, +9^{\circ}35'20''$. North is at the top and east is to the left. *Right*: Magnified region surrounding the micro cluster. [See the electronic edition of the *Journal* for a color version of this figure.]

that the 24 μm sources represented collapsing, fragmenting filaments.

The brightest of these cores in the submillimeter is IRAS 12 S1, located near the position of the Cohen et al. (1985) secondary peak. IRAS 12 S1 also corresponds to the millimeter source D-MM1 in the survey of Peretto et al. (2006). Wolf-Chase et al. (2003) suggested that IRAS 12 S1 is an intermediate-mass Class 0 protostar. In this paper we present *Spitzer* and Magellan observations that demonstrate that S1 is, in fact, a complex of extremely young objects.

2. NEW OBSERVATIONS

2.1. *Spitzer* Observations

NGC 2264 was observed with IRAC (Fazio et al. 2004) on 2004 March 6. The observations were conducted in High Dynamic Range mode, with integration times of 0.4 and 10.4 s per frame. Three integrations were taken at each dithered position, yielding a typical total integration time of 31 s per point. The grid was laid out in a 7×11 pattern with $290''$ offsets, resulting in a total coverage area of approximately $33' \times 51'$. The map was centered at $6^{\text{h}}40^{\text{m}}54^{\text{s}}.92, +9^{\circ}37'7''.94$, with a position angle of -1.5° . In High Dynamic Range mode, each position has both long and short integrations to allow the nonsaturating measurement of both bright and faint sources. The standard Basic Calibrated Data from the *Spitzer* Science Center were mosaicked using IRAF routines, and source photometry was obtained using DAOPHOT and IDL.

The MIPS (Rieke et al. 2004) observations were conducted on 2004 March 16 using the scan map mode. Fourteen scan legs of $0.75'$ length and $160''$ offsets were taken at medium speed. Total integration times of 80 and 40 s per point were obtained in the 24 and 70 μm bands, respectively. We also obtained sparse coverage in the 160 μm band, but most of the data were saturated due to the extremely high backgrounds in the molecular cloud. The full map was centered at $6^{\text{h}}40^{\text{m}}55^{\text{s}}, +9^{\circ}37'8''$, with a position angle of 179° . These observations were processed with the MIPS Data Analysis Tool (DAT; Gordon et al. 2005), which produces calibrated mosaics of the mapped regions. Processing of the resultant image products to obtain photometry was done using standard routines in DAOPHOT and IDL.

For this paper, we utilize a magnitude scale based on the spectral energy distribution of an A0 star. The magnitude zero points for the 3.6, 4.5, 5.8, 8.0, and 24 μm bands are 277.5, 179.5, 116.6, 63.1, and 7.3 Jy, respectively.

2.2. Magellan Observations

Near-infrared imaging of the IRAS 12 S1 region was obtained with the PANIC camera on the 6.5 m Baade telescope (Martini et al. 2004) at Las Campanas Observatory. The PANIC camera uses a 2.5 μm cutoff HAWAII-1 HgCdTe array with a scale of $0''.125$ per pixel. Images were taken in the J , H , and K_s bands as well as in a narrowband molecular hydrogen filter centered on the 2.12 μm 1–0 $S(1)$ line. The broadband images were obtained on 2004 December 30 with a total integration time of 900 s in each band. The molecular hydrogen observations were taken on 2005 February 23 with a total integration time of 2400 s. Photometric calibration of PANIC images was done using a suite of 2MASS sources detected in the images. The observations were obtained under excellent conditions, with a stellar FWHM of $0''.37$ for the December observations and $0''.44$ for the February run. Processing of the PANIC images was done with IRAF scripts developed for that instrument by S. E. Persson and P. Martini, and source photometry was done with standard DAOPHOT routines. Point-source photometry was obtained with fitting of an empirical point spread function.

3. RESULTS

Figure 1 is a color composite image of the IRS 2 region utilizing both IRAC and MIPS data. The color coding is blue = 3.6 μm , green = 8.0 μm , and red = 24 μm . We have chosen this combination of bands to highlight the different kinds of physical objects in the region. The 3.6 μm emission is dominated by stellar photospheres, and the majority of the sources found in this band are also detected in the near-infrared at 2MASS sensitivities. The 8 μm emission is associated with hot dust, and for a region as young as NGC 2264, most of the 8 μm emitters are T Tauri stars. There can also be a substantial extended component to the 8 μm emission that is due to the strong PAH band at this wavelength. Finally, the 24 μm band is particularly useful for identifying the Class I and Class 0 objects—protostars with significant circumstellar disks and envelopes.

The emission in the region is dominated by IRS 2. The source consists of an unresolved component, present at all wavelengths and an extended component that is particularly prominent at 8 μm . The 24 μm emission highlights the coldest and presumably youngest objects in the region. They appear to be aligned like the spokes of a wheel. This overall morphology and its relationship with the dense cloud detected at submillimeter wavelengths is discussed in detail in the paper by Teixeira et al. (2006).

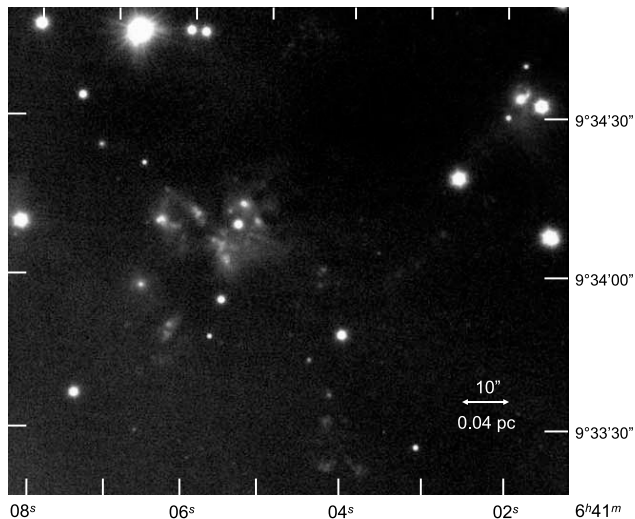


FIG. 2.— Composite image of PANIC data for the IRAS 12 S1 core region. [See the electronic edition of the *Journal* for a color version of this figure.]

The present paper focuses on the very dense collection of sources denoted by “core” in Figure 1. In the IRAC observations at 3.6, 4.5, 5.8, and 8.0 μm , the sources are somewhat confused given the angular resolution of approximately $2''$ afforded by *Spitzer* at IRAC wavelengths. We are still able to discern at least 10 distinct sources at 3.6 μm within a diameter of $20''$, which at the assumed distance of NGC 2264 corresponds to only 0.08 pc. The implied stellar density is greater than $4 \times 10^4 \text{ pc}^{-3}$.

Figure 2 shows a JHK_s color composite taken with the PANIC camera. The image covers the $1'.8 \times 1'.6$ box indicated on Figure 1. Both the core cluster and a small surrounding region are included in the image. The excellent seeing in the PANIC observations reveals a complicated mixture of point sources, extended emission, and obscuration bands. Figure 3 shows the image of the same region taken in the 2.12 μm molecular hydrogen line. We have performed a crude continuum correction by subtracting a K_s -band image that has been scaled by the relative bandwidths of the filters. While this subtraction is good enough to identify pure molecular hydrogen features, it is inaccurate for identifying continuum sources that also emit in H_2 . We find that there are extended regions of H_2 emission, particularly to the west of the core.

Photometry from the *Spitzer* and PANIC observations is presented in Table 1. The source list covers the region shown in the PANIC image. Given the very wide range of angular resolution in this data set (from FWHM of $0''.37$ for the PANIC images to $7''$ for the 24 μm band), it is not possible in every case to unambiguously assign the appropriate long wavelength flux to each PANIC source. When possible, we use data from the PANIC data for JHK_s magnitudes. Sources brighter than $J = 12$, $H = 12$, and $K_s = 11$ are saturated, and we substitute 2MASS photometry. Sources detected in the PANIC observations are indicated in Figure 4 with numbers below 100. Sources detected only in the *Spitzer* images have numbers greater than 1000.

4. DISCUSSION

The simulations of Bate et al. (2003) and Bate & Bonnell (2005) follow the collapse of a Jeans-unstable turbulent core. They show that star formation commences on timescales comparable to the global free-fall time, and it proceeds by forming dense cores that fragment into stars and brown dwarfs. Dynamical interactions are important in the development of the ensemble. More recently, Kurosawa et al. (2004) have simulated the

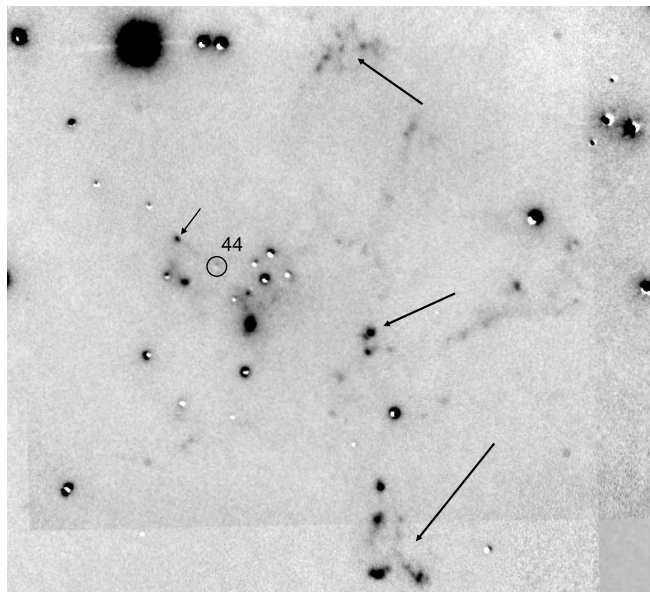


FIG. 3.— Continuum-subtracted narrowband image of the IRAS 12 S1 core in molecular hydrogen $S(1) 2.12 \mu\text{m}$. A prominent series of H_2 knots is indicated by the arrows. Source 44 (see text) is indicated, as well as an apparently associated molecular hydrogen knot.

appearance of the Bate et al. (2003) simulations in the *Spitzer* bands. We argue that the S1 stars represent just such a fragmenting core. For this hypothesis to be plausible, it is necessary to demonstrate the extreme youth of the objects.

Figure 4 is a K_s PANIC image of the S1 region with the sources identified. Overlaying the image are the 850 μm contours from Wolf-Chase et al. (2003). As shown in the figure, the “microcluster” is located precisely at the peak of the IRAS 12 S1 submillimeter source mapped by Wolf-Chase et al. (2003) (also denoted Core C by Williams & Garland 2002). The entire core has a composite spectral energy distribution (SED) that peaks in the far-infrared. Wolf-Chase et al. (2003) derived an envelope mass of $17.6 M_\odot$ within a $28''$ diameter. Based on the ratio of submillimeter to bolometric luminosity, they classified S1 as an intermediate-mass Class 0 protostar. Williams & Garland (2002) observed the region in HCO^+ and detected an emission line with a strong, redshifted absorption feature. They interpreted this spectral signature as indicative of infall. Hence, both continuum and line observations suggest that IRAS 12 S1 is undergoing active collapse. The submillimeter contours of Wolf-Chase et al. (2003) show that S1 is somewhat extended but unresolved at both 850 and 450 μm . Rather than being a single protostar, however, it is clear from the new shorter wavelength observations that S1 is made up of a cluster of discrete sources.

Figure 5 shows the SEDs of the sources encompassed by the submillimeter peak. Except for 34, which appears to be an unreddened foreground star, all the sources are steeply rising to longer wavelengths and can be classified as Class 0 or Class I. While all these stars appear to have significant amounts of circumstellar matter, it is not possible to unambiguously assign the relative contributions of the stars to the 24 μm flux since in many cases the sources are badly confused. For example, the flux given to 38 really is a composite that can include contributions from 41 and others.

The SEDs in S1 are markedly different from those just outside the dense submillimeter core. Figures 6 and 7 show the SEDs for the regions $1'$ west and $1'$ northeast of S1, respectively. There are a number of flat SEDs in those two adjacent regions, but the

TABLE 1
SOURCES IN THE IRAS 12 S1 CORE

Star ID	R.A. (J2000.0)	Decl. (J2000.0)	2MASS Name	<i>J</i>	<i>H</i>	<i>K</i>	[3.6 μ m]	[4.5 μ m]	[5.8 μ m]	[8.0 μ m]	[24 μ m]
2.....	06 41 01.32	+09 34 52.7	06410133+0934526	12.91	12.83	12.46	11.94	11.71	11.40	10.44	6.49
3.....	06 41 01.37	+09 34 07.7	...	13.20	12.96	12.34
4.....	06 41 01.42	+09 34 08.0	06410141+0934081	12.35	11.71	11.61	11.40	11.40	11.28	10.97	9.03
6.....	06 41 01.56	+09 34 32.9	06410156+0934329	14.40	12.64	11.38	10.05	9.69	9.05	8.24	...
7.....	06 41 01.75	+09 34 40.4	...	20.25	17.26	15.50	13.52	12.78	12.12
8.....	06 41 01.78	+09 33 34.6	18.69	16.02	15.85
9.....	06 41 01.82	+09 34 34.0	06410182+0934342	17.08	13.80	11.67	9.31	8.61	7.76	6.99	2.93 ^a
10.....	06 41 01.97	+09 34 30.7	16.49	14.61	12.37	11.19
1332.....	06 41 02.18	+09 34 14.5	15.95	14.23	13.56
1334.....	06 41 02.21	+09 34 30.0	11.29
11.....	06 41 02.52	+09 34 55.9	06410253+0934557	12.58	11.82	11.62	11.61	11.67	11.61	11.42	...
1349.....	06 41 02.54	+09 35 02.0	16.33
1352.....	06 41 02.57	+09 34 42.6	14.55
13.....	06 41 02.59	+09 34 18.8	06410258+0934190	12.61	12.11	11.89	11.91	11.99	11.98	12.03	...
1374.....	06 41 02.81	+09 34 08.0	15.76	14.37	13.57
15.....	06 41 03.07	+09 33 27.4	...	16.96	16.14	15.78	15.57	15.68
1388.....	06 41 03.07	+09 34 03.0	14.80	13.55
1392.....	06 41 03.19	+09 32 55.0	06410319+0932550	14.44	13.76	13.36	12.76	12.59	12.33	11.69	...
17.....	06 41 03.60	+09 34 53.0	18.03	16.14	14.23	13.59	13.15
16.....	06 41 03.60	+09 34 04.4	18.11	16.37	15.90
18.....	06 41 03.79	+09 34 53.8	...	16.74	15.87	15.54
1424.....	06 41 03.82	+09 33 23.0	15.59	14.18	13.50
1425.....	06 41 03.86	+09 35 03.8	13.27
1427.....	06 41 03.89	+09 34 32.9	16.64	15.42	13.85
1432.....	06 41 03.98	+09 35 03.1	7.57
1433.....	06 41 03.98	+09 33 18.0	15.47
19.....	06 41 04.06	+09 33 48.6	06410405+0933486	15.16	13.58	12.90	12.47	12.42	12.32	12.24	...
1438.....	06 41 04.13	+09 33 01.4	06410411+0933018	10.17	10.22	10.22	10.28	10.32	10.38	10.19	...
20.....	06 41 04.15	+09 34 57.0	06410417+0934572	14.83	14.05	13.68
21.....	06 41 04.20	+09 33 37.1	16.67	15.29	13.68	13.26
22.....	06 41 04.20	+09 33 23.8	...	12.58	...	17.02	14.89	13.42	12.46	11.20	...
1444.....	06 41 04.22	+09 33 32.0	15.50	14.18	13.16	11.87	...
23.....	06 41 04.25	+09 34 59.5	15.85	12.44	9.48	8.57	7.57	7.04	3.07
1445.....	06 41 04.25	+09 34 52.0	12.30
1448.....	06 41 04.25	+09 34 45.5	14.37	12.76
24.....	06 41 04.30	+09 34 00.8	17.14	15.40	14.58	13.63
1460.....	06 41 04.37	+09 32 57.1	06410436+0932576	12.75	15.09	12.68	14.30	14.14	14.23
1459.....	06 41 04.37	+09 33 59.4	15.57
26.....	06 41 04.46	+09 33 43.6	18.91	16.27	14.29	13.55	12.75	11.65	7.22
1465.....	06 41 04.46	+09 34 50.5	14.83
1470.....	06 41 04.58	+09 34 47.6	15.41
1473.....	06 41 04.63	+09 33 54.4	15.24
1474.....	06 41 04.63	+09 34 58.1	10.44
1476.....	06 41 04.70	+09 33 48.6	16.29
1478.....	06 41 04.70	+09 34 54.8	13.31
1481.....	06 41 04.78	+09 34 43.3	15.93	14.10
1485.....	06 41 04.85	+09 35 03.5	14.61
1492.....	06 41 05.06	+09 33 00.0	06410505+0933002	14.13	13.37	13.16	12.88	12.98	12.86	12.46	...
30.....	06 41 05.16	+09 34 10.2	17.42	15.16	12.05	10.83	9.94	9.07	...
33.....	06 41 05.35	+09 33 13.3	06410536+0933134	12.58	11.85	11.64	11.41	11.55	11.38	11.38	...
32.....	06 41 05.35	+09 34 13.4	06410535+0934133	19.42	16.09	13.95	11.69	10.91	9.71
1512.....	06 41 05.40	+09 33 23.4	16.52	15.86
34.....	06 41 05.42	+09 34 09.5	06410542+0934095	14.66	13.77	13.48	13.25
35.....	06 41 05.50	+09 34 11.6	15.63	11.85	...	9.68	8.92	...
1515.....	06 41 05.50	+09 34 36.8	15.40
36.....	06 41 05.52	+09 35 01.3	16.56	15.00	13.88	13.70	13.27	12.60	...
38.....	06 41 05.57	+09 34 08.0	16.02	11.73	10.43	9.40	8.74	2.21 ^b
39.....	06 41 05.62	+09 33 55.1	06410562+0933549	16.72	14.63	13.33	11.82	11.23	10.60	9.77	...
41.....	06 41 05.74	+09 34 06.2	19.01	15.07	11.73	10.47	9.46	8.71	...
42.....	06 41 05.76	+09 33 47.9	...	17.88	16.82	16.12	14.87	14.06	13.05
1530.....	06 41 05.76	+09 33 00.4	16.21	15.33	14.48
1542.....	06 41 05.86	+09 34 52.7	14.23
43.....	06 41 05.88	+09 34 45.8	...	16.75	13.66	12.15	11.18	11.00	10.87	10.65	...
44.....	06 41 05.93	+09 34 11.3	06410598+0934115	...	17.35	15.30	12.90	11.75	10.73	9.44	3.8 ^c

TABLE 1—Continued

Star ID	R.A. (J2000.0)	Decl. (J2000.0)	2MASS Name	<i>J</i>	<i>H</i>	<i>K</i>	[3.6 μ m]	[4.5 μ m]	[5.8 μ m]	[8.0 μ m]	[24 μ m]
45.....	06 41 05.93	+09 34 04.8	19.97	10.29	8.68	...
1547.....	06 41 05.93	+09 35 03.1	13.78	13.49	13.37	11.89	...
1549.....	06 41 05.95	+09 34 39.7	13.36
46.....	06 41 06.05	+09 34 46.2	06410604+0934461	16.40	13.58	12.25	11.39	11.18	10.99	10.60	...
47.....	06 41 06.17	+09 34 08.8	15.86	12.51	10.58	9.83	9.19	...
1561.....	06 41 06.24	+09 33 08.6	06410623+0933087	14.11	13.35	13.05	12.55	12.44	12.39	12.22	...
48.....	06 41 06.29	+09 33 50.0	06410629+0933496	...	19.04	16.73	11.44	10.06	8.90	7.91	3.33
1568.....	06 41 06.34	+09 34 15.2	12.97	11.08
49.....	06 41 06.38	+09 34 10.2	06410642+0934099	...	16.44	14.48	12.59
1576.....	06 41 06.41	+09 35 06.0	06410640+0935061	16.42	15.95	15.22	15.31	14.87
1579.....	06 41 06.43	+09 33 43.2	14.87	13.52	12.81
1588.....	06 41 06.60	+09 35 00.2	12.15	...
1591.....	06 41 06.60	+09 35 02.0	13.56
51.....	06 41 06.62	+09 34 21.0	...	19.16	16.89	15.55	14.15	13.66	12.75	11.59	...
52.....	06 41 06.65	+09 33 57.6	06410665+0933576	...	16.99	13.87	11.57	10.73	9.98	9.12	5.1
1597.....	06 41 06.65	+09 34 26.4	16.81	15.02
53.....	06 41 06.70	+09 33 29.9	17.06	13.70	12.61
1600.....	06 41 06.72	+09 34 37.9	11.88
1601.....	06 41 06.72	+09 34 31.8	14.42	14.42
54 ^d	06 41 06.74	+09 34 45.8	06410673+0934459	11.76	10.28	9.23	8.39	7.80	6.69	5.72	1.82
1603.....	06 41 06.74	+09 34 59.2	14.29
1604.....	06 41 06.74	+09 34 53.8	11.18
1607.....	06 41 06.77	+09 33 34.6	12.06	9.45	8.70	8.47	3.54
1610.....	06 41 06.82	+09 35 02.4	13.61
1622.....	06 41 07.10	+09 34 42.2	8.37	...	8.42
1623.....	06 41 07.13	+09 34 44.8	8.35
55.....	06 41 07.20	+09 34 24.2	06410719+0934242	...	17.93	14.81	13.16	12.67	12.34	12.13	...
1630.....	06 41 07.22	+09 34 41.2	12.35
1637.....	06 41 07.34	+09 34 40.4	12.10
56.....	06 41 07.39	+09 34 54.8	06410740+0934549	18.52	14.48	12.09	10.25	9.64	9.27	8.68	...
57.....	06 41 07.44	+09 34 33.6	06410744+0934335	15.20	14.24	13.98	13.80	13.66	13.42
58.....	06 41 07.49	+09 33 37.1	06410748+0933369	14.43	13.42	13.07	12.69	12.46	12.09	11.28	...
1656.....	06 41 07.68	+09 34 19.2	13.57	11.19	10.03	9.16	4.29
1665.....	06 41 07.92	+09 33 33.8	14.70
1666.....	06 41 07.92	+09 34 27.8	15.32
1667.....	06 41 07.92	+09 34 33.6	16.04
60.....	06 41 07.97	+09 34 46.9	06410798+0934469	13.97	12.53	12.06	11.05	10.57	10.20	9.41	...
1669.....	06 41 07.97	+09 34 16.3	13.53
61.....	06 41 08.06	+09 33 13.3	...	19.05	17.91	17.87	17.42
1675.....	06 41 08.11	+09 34 30.0	16.44	15.12
1677.....	06 41 08.14	+09 34 16.0	13.26
62.....	06 41 08.21	+09 34 09.5	06410821+0934094	13.13	11.90	11.41	10.95	10.65	10.26	9.33	5.25 ^e
63.....	06 41 08.28	+09 34 06.6	17.03	11.8	...
1683.....	06 41 08.33	+09 34 25.7	15.08
64.....	06 41 08.54	+09 34 13.1	06410854+0934132	16.32	13.23	11.59	10.95	10.74	10.45	10.06	...
1690.....	06 41 08.57	+09 34 08.0	12.53

NOTE.—Units of right ascension are hours, minutes, and seconds, and units of declination are degrees, arcminutes, and arcseconds.

^a The 24 μ m flux is confused and contains contributions from source 10.

^b The 24 μ m flux is confused and contains contributions from sources 30, 32, 34, 35, 37, 40, and 41.

^c The 24 μ m flux is confused and contains contributions from sources 47 and 49.

^d Source 54 is V 608 Mon.

^e The 24 μ m flux is confused and contains contributions from the nearby source 63, which has the more steeply rising SED.

majority of the detected objects have SEDs consistent with highly reddened low-mass stars.

A second indication of the youth of the microcluster is the presence of extensive molecular hydrogen flows. In the S1 core itself, several knots of molecular hydrogen are present, for example, between sources 47 and 49 and between sources 40 and 37. The most extensive molecular hydrogen line emission is away from the core, however. A north-south series of knots (indicated by the arrows in Figure 3) is quite prominent in the continuum subtracted H₂ image. The morphology is reminiscent of bipolar Herbig-Haro flows. However, we find no evidence for any can-

didate sources at 24 or 70 μ m other than possibly 26. It is a relatively weak flat-spectrum source with no significant emission at 70 μ m. It is possible that one of the Class I sources in the microcluster is the source of the H₂ emission, although that interpretation would be difficult to reconcile with the north-south geometry of the knots. That possibility will likely require proper motion studies of the knots to prove conclusively.

A number of the sources appear to have opaque dust lanes that are likely caused by circumstellar disks. The best example is 44, which has a distinctly bipolar appearance. Moreover, this source is associated with molecular hydrogen emission that

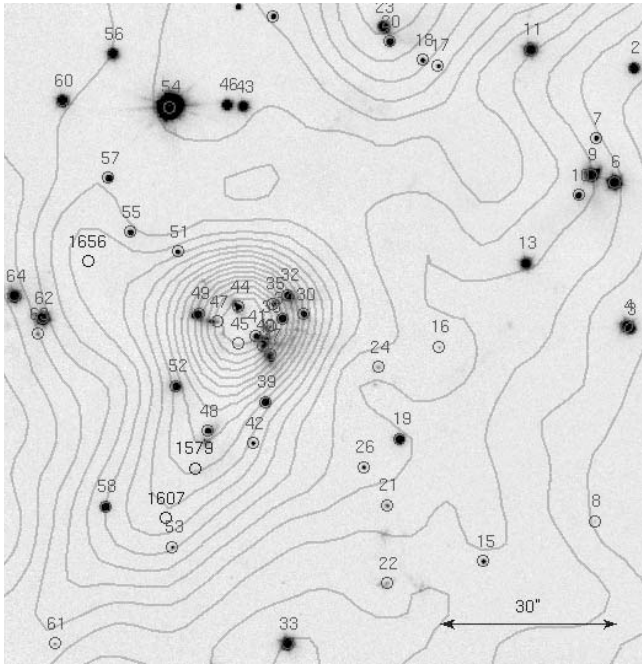


FIG. 4.—PANIC *K*-band image of the core region. Source numbers are indicated, with sources detected only in the *Spitzer* images having numbers greater than 1000. The contours are from 850 μm continuum SCUBA archival data (Wolf-Chase et al. 2003). The contour intervals are 0.1 Jy beam⁻¹. [See the electronic edition of the *Journal* for a color version of this figure.]

emanates from the “pole” and terminates in a bright knot 7'' to the northeast.

An upper limit to the age of the S1 group can be determined from dynamical arguments. The characteristic nonthermal velocity dispersion of the gas in the core has been measured by Williams & Garland (2002) to be 0.7–1.0 km s⁻¹. Williams & Garland (2002) also identified five other submillimeter cores in the main S1 complex. The measured core to core velocity dispersion is 0.9 km s⁻¹. If we adopt a 0.7 km s⁻¹ one-dimensional dispersion for the stars, the dispersal time in the S1 microcluster is only 40,000 yr for a 10'' radius. The 0.7 km s⁻¹ velocity dispersion may, in fact, be an underestimate if we consider velocity dispersions found in other star formation regions. For example, Jones & Walker (1988) measured a one-dimensional dispersion of 2 km s⁻¹ for the Orion nebula stars. The simulations of tur-

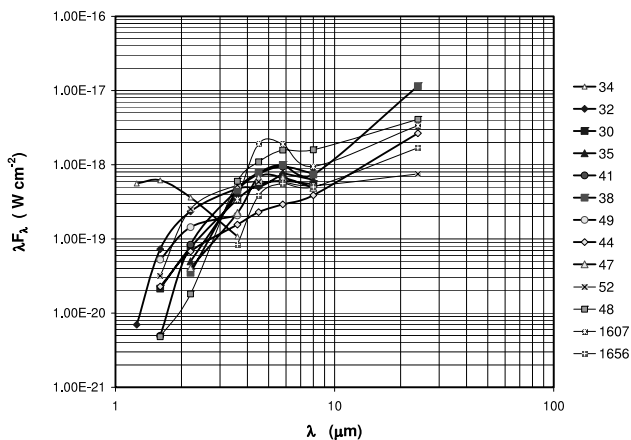


FIG. 5.—Spectral energy distributions for sources in the S1 core. The legend numbers refer to the star ID given in Table 1. [See the electronic edition of the *Journal* for a color version of this figure.]

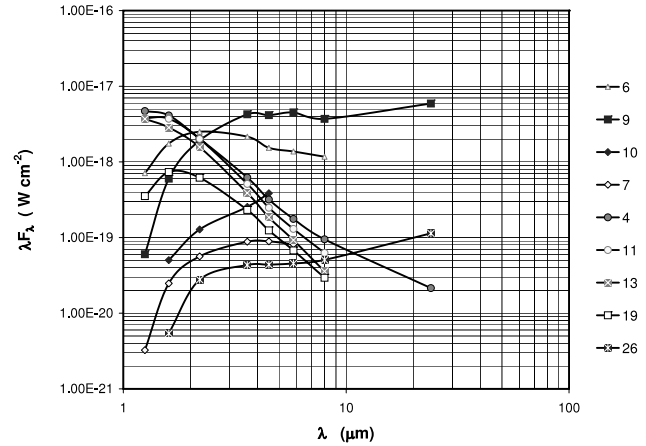


FIG. 6.—Spectral energy distributions for sources west of the S1 core. The legend numbers refer to the star ID given in Table 1. [See the electronic edition of the *Journal* for a color version of this figure.]

bulent core collapse exhibit many examples of dynamical interactions between the forming stars. In particular, the lower mass members often attain a high enough velocity to be ejected from the core region. Bate & Bonnell (2005) found one-dimensional velocity dispersions between 1 and 2.5 km s⁻¹, depending on initial conditions. Hence, our use of 0.7 km s⁻¹ for the velocity dispersion is likely to be conservative.

What can be said about the masses of the members of the microcluster? Unfortunately, the wide range of parameters afforded by extinction (both disk and envelope), inclination, and accretion rate makes fitting of individual sources to evolutionary models problematic. Limits can be established, however, if we consider the ensemble properties of the microcluster. Wolf-Chase et al. (2003) derive an envelope mass of 17.6 M_{\odot} and a bolometric luminosity of 107.5 L_{\odot} , leading to their association of the source with an intermediate-mass protostar. The *Spitzer* observations show, however, that the luminosity is actually shared by perhaps a dozen lower mass objects. For extremely young objects, the far-infrared and submillimeter luminosity is expected to be a valid measure of the bolometric luminosity since they will still be surrounded by envelopes that intercept the bulk of the short wavelength emission. If we apply the pre-main-sequence tracks of Siess et al. (2000), a star with a luminosity of 10 L_{\odot} corresponds to a mass of only 0.9 M_{\odot} at an age of 10⁵ yr. Thus, we may be seeing the fragmentation of a molecular core into solar or lower mass stars.

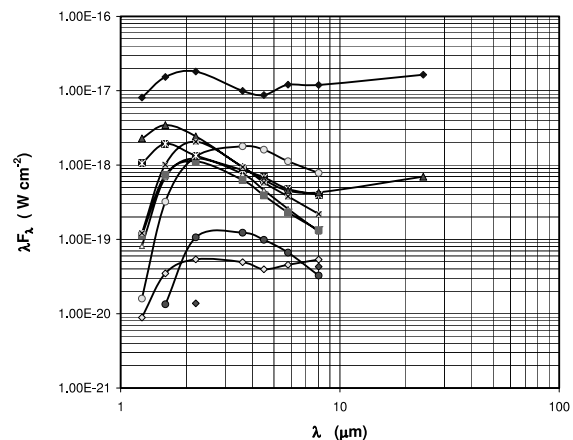


FIG. 7.—Spectral energy distributions for sources northeast of the S1 core. The legend numbers refer to the star ID given in Table 1. [See the electronic edition of the *Journal* for a color version of this figure.]

5. SUMMARY

As part of a larger program surveying young clusters, we have mapped the star-forming region NGC 2264 with the MIPS and IRAC instruments on *Spitzer*. We have found a remarkable collection of extremely young objects in the IRS 2 region (Teixeira et al. 2006). One of these objects, associated with the submillimeter source IRAS 12 S1, proves to be a dense collection of protostellar objects in its own right. Based on the steeply rising SEDs of the objects, the proximity of molecular hydrogen outflows, and a dynamical age of less than 40,000 yr, we argue that this “micro cluster” may represent a fragmenting, collapsing core, very much as simulated by Bate et al. (2003).

This work is based on observations made with the *Spitzer* Space Telescope, which is operated by the Jet Propulsion Laboratory, California Institute of Technology under NASA contract 1407. Support for this work was provided by NASA through Contract Number 960785 issued by JPL/Caltech. This work made use of Simbad and 2MASS databases as well as IRAF, ds9, and the IDL Astronomy Library. P. Teixeira acknowledges support from the scholarship SFRH/BD/13984/2003 awarded by the Fundacao para a Ciência e Tecnologia (Portugal). This paper includes data gathered with the 6.5 m Magellan Telescopes located at Las Campanas Observatory, Chile.

Facilities: Spitzer, Magellan:Baade

REFERENCES

- Bate, M. R., & Bonnell, I. 2005, MNRAS, 356, 1201
 Bate, M. R., Bonnell, I., & Bromm, V. 2003, MNRAS, 339, 577
 Castelaz, M. W., & Grasdalen, G. 1988, ApJ, 335, 150
 Cohen, M., Harvey, P. M., & Schwartz, R. D. 1985, ApJ, 296, 633
 Dahm, S. E., & Simon, T. 2005, AJ, 129, 829
 Fazio, G. G., et al. 2004, ApJS, 154, 10
 Flaccomio, E., Micela, G., Sciortino, S., Favata, F., Corbally, C., & Tomaney, A. 1999, A&A, 345, 521
 Gordon, K., et al. 2005, PASP, 117, 503
 Herbig, G. H. 1954, ApJ, 119, 483
 Jones, B. F., & Walker, M. F. 1988, AJ, 95, 1755
 Kurosawa, R., Harries, T., Bate, M. R., & Symington, N. H. 2004, MNRAS, 351, 1134
 Margulis, M., Lada, C. J., & Snell, R. L. 1988, ApJ, 333, 316
 Margulis, M., Lada, C. J., & Young, E. T. 1989, ApJ, 345, 906
 Martini, P., Persson, S. E., Murphy, D. C., Birk, C., Schettmann, S. A., Gunnels, S. M., & Koch, E. 2004, Proc. SPIE, 5492, 1653
 Park, B., Sung, H., Bessell, M. S., & Kang, Y. H. 2000, AJ, 120, 894
 Peretto, N., André, Ph., & Belloche, A. 2006, A&A, 445, 979
 Rebull, L. M., et al. 2002, AJ, 123, 1528
 Rieke, G. H., et al. 2004, ApJS, 154, 25
 Sargent, A. I., Van Duinen, R. J., Nordh, H. L., Fridlund, C. V. M., Aalders, J. W. G., & Beintema, D. 1984, A&A, 135, 377
 Schwartz, P. R., Thronson, H. A., Odenwald, S. F., Glaccum, W., Loewenstein, R. F., & Wolf, G. 1985, ApJ, 292, 231
 Siess, L., DuFour, E., & Forestini, M. 2000, A&A, 358, 593
 Sung, H., Bessell, M. S., & Lee, S. W. 1997, AJ, 114, 2644
 Teixeira, P. S., et al. 2006, ApJ, 636, L45
 Walker, M. F. 1956, ApJS, 2, 365
 Williams, J. P., & Garland, C. A. 2002, ApJ, 568, 259
 Wolf-Chase, G., Moriarty-Schieven, G., Fich, M., & Barsony, M. 2003, MNRAS, 344, 809
 Wolf-Chase, G. A., & Walker, C. K. 1995, ApJ, 447, 244